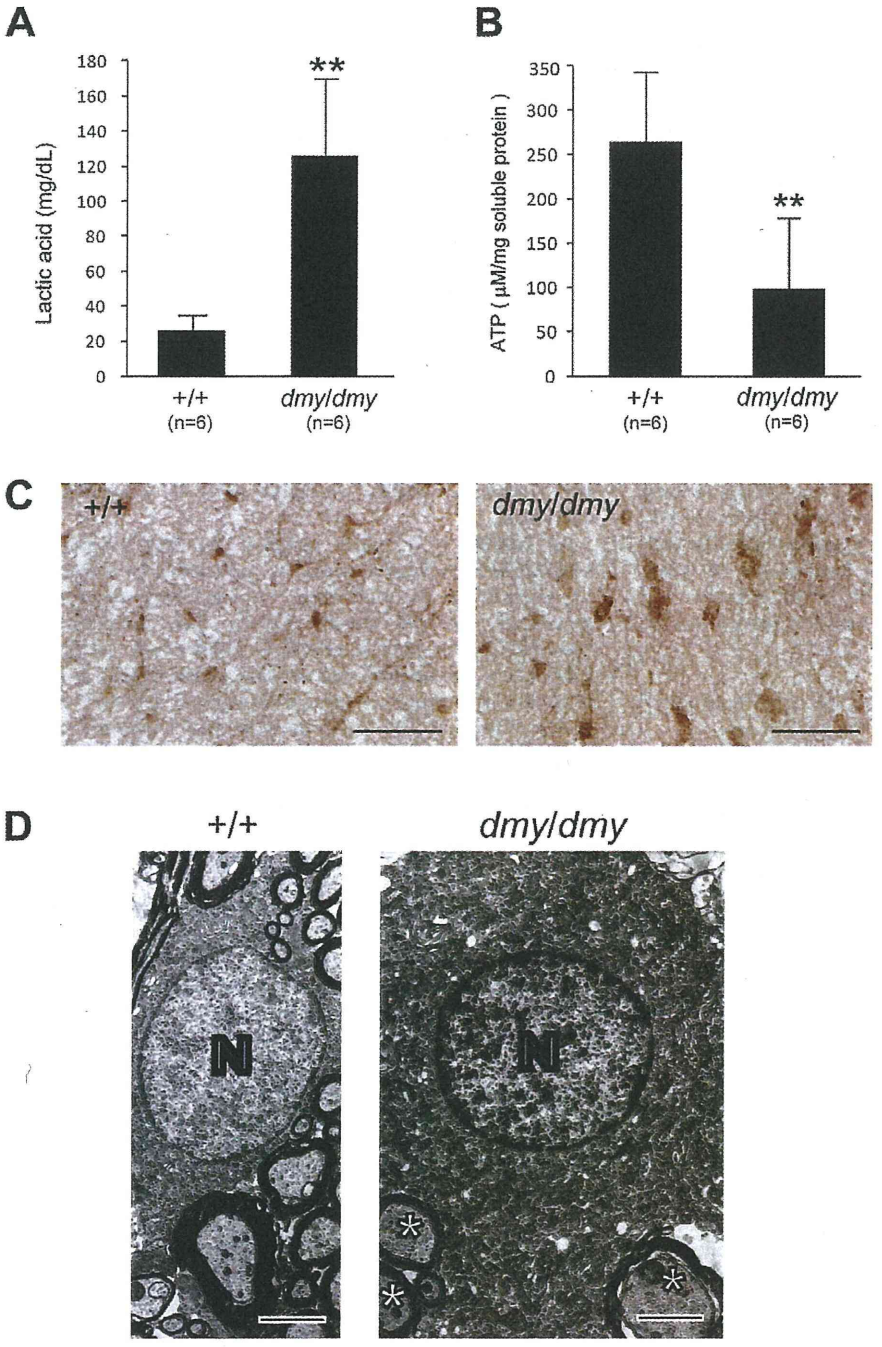

Figure 3. Biochemical and morphological abnormalities in the mitochondria of *dmy/dmy* mutant rats. A. Lactic acid concentration in cerebrospinal fluid of 6–7-week-old *dmy/dmy* rats and age-matched wild-type rats. **, P<0.002. B. ATP levels in the brain of 6–7-week-old *dmy/dmy* rats and age-matched wild-type rats. **, P<0.005. C. Cytochrome oxidase staining of the spinal cords of 6–7-week-old *dmy/dmy* (right) and age-matched wild-type (left) rats. Swollen oligodendrocytes were often seen they showed increased COX reaction product. Bar = 50 µm. D. Electron microphotographs of a swollen oligodendrocyte in a *dmy/dmy* rat (right) and an oligodendrocyte in a control wild-type rat. White matter of thoracic spine at 6 weeks of age. N: Nucleus of the oligodendrocyte. Axons adjacent to the oligodendrocyte are indicated by asterisks. Bar = 2 µm.
doi:10.1371/journal.pgen.1001262.g003

across tissues would provide a molecular framework to relate mitochondrial biology and pathogenesis [27].

A point concerning *Mrs2* gene expression in the CNS that is worth noting after our experiments and observations is that the gene in question is expressed at a higher rate in neurons than in oligodendrocytes (Figure 4, Figure S3). This was rather unexpected if we consider that oligodendrocytes are the cells actually responsible for myelination of the CNS. At this time, it remains

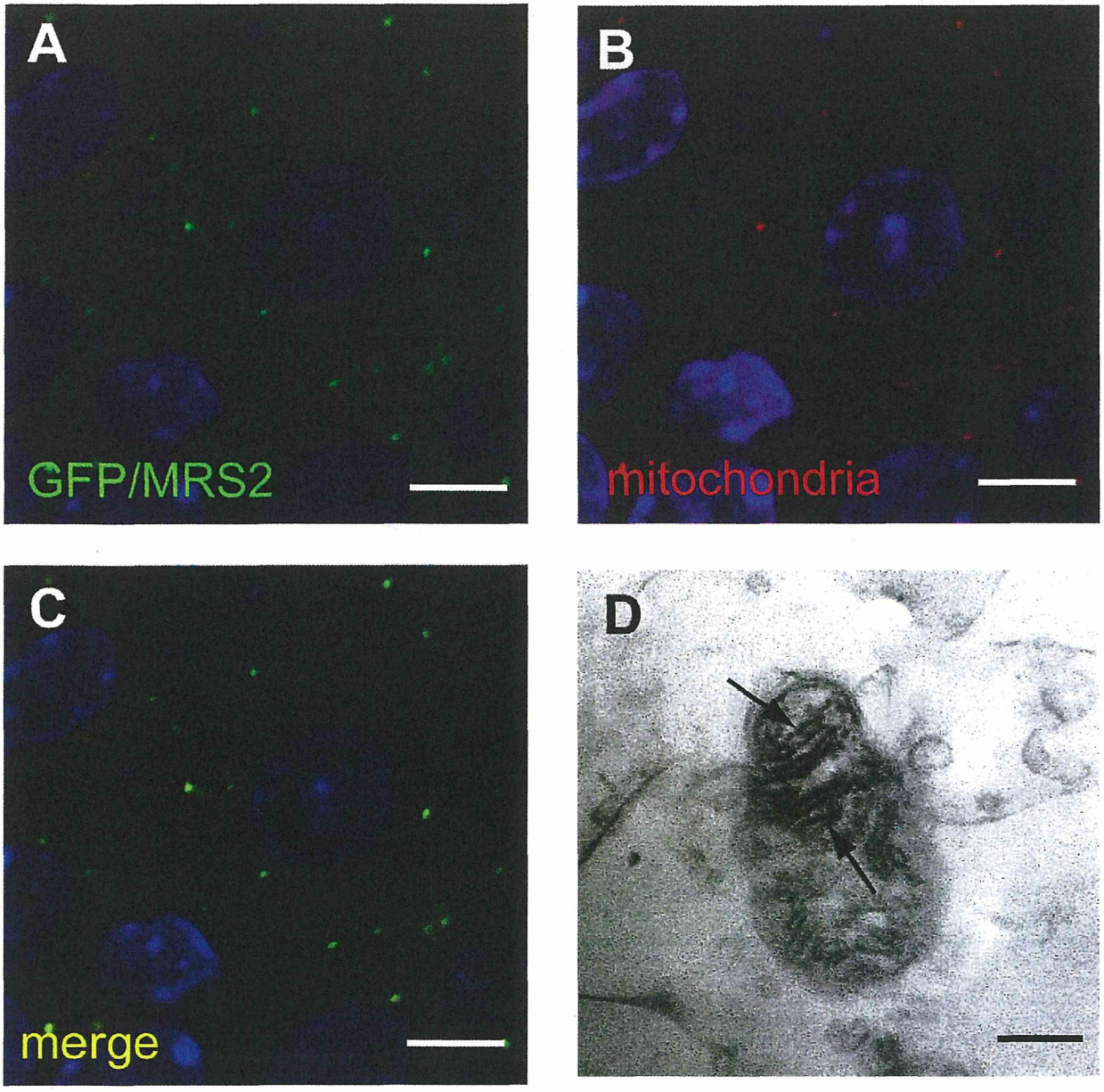

Figure 4. Expression of MRS2 protein in the mitochondria. MRS2-GFP recombinant protein (Green) was seen in the cytoplasm of pyramidal cells (A). MRS2-GFP signals were colocalized with the mitochondria (B), as shown in the confocal image of GFP and mitochondrial immunohistochemistry (C). Nuclei were stained with DAPI (Blue). Bar: 5 μm. Immunoelectron microscopy using anti-GFP antibody revealed that MRS2-GFP signals were localized in the inner membrane of the mitochondria (arrows) (D). Bar: 200 nm.
doi:10.1371/journal.pgen.1001262.g004

unclear whether the demyelination in *dmy/dmy* rats is triggered cell-autonomously or cell-nonautonomously. Instead, it is likely that demyelination is enhanced by the surrounding cells, such as activated microglia and astroglia. At 6 weeks of age, when *dmy/dmy* rats began to exhibit ataxia [9], cytokine levels were elevated and microglia were activated (Figure 5), and it is considered that activated microglia cause neuronal damage through the release of potentially cytotoxic molecules, such as proinflammatory cytokines, reactive oxygen intermediates, proteinases, and complement proteins [28]. Oligodendrocytes show greater vulnerability to such molecules [29,30]. Additionally, Kuwamura and co-workers reported prominent astrogliosis and many ED-1-positive macrophages in myelin-destroyed areas [9]. When considered together, these morphological observations led us to believe that the demyelination observed in *dmy/dmy* rats is probably enhanced by activated microglia and astroglia.

In summary, we identified $Mrs2^{dmy}$ as a loss-of-function mutation of the *Mrs2* gene that normally encodes Mg^{2+} transporter protein of the mitochondrial inner membrane. Our observations also demonstrate that the mechanisms underlying the

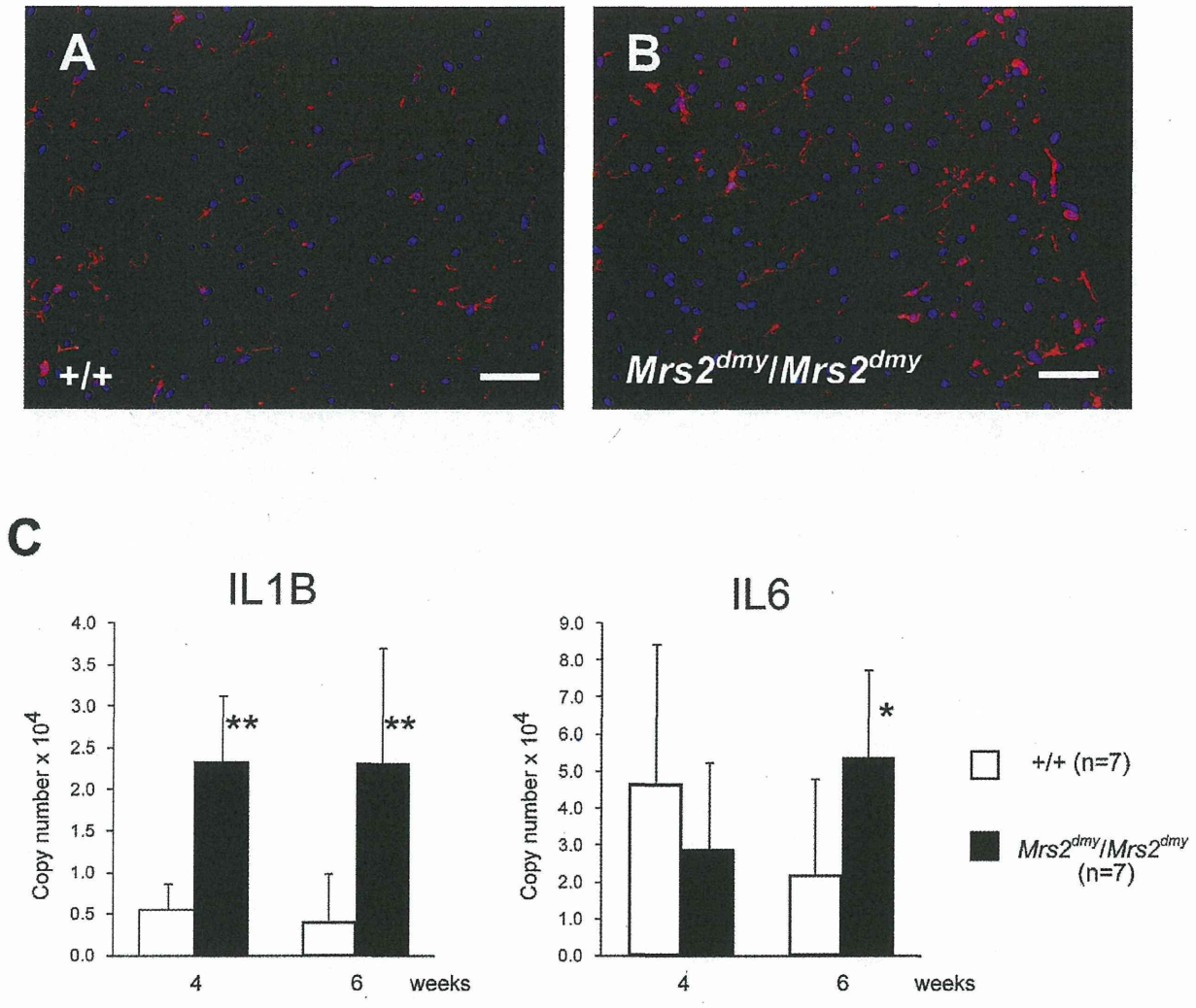

Figure 5. Activation of microglia in the central nervous system of *Mrs2*^{dmy}/*Mrs2*^{dmy} rats. Immunohistochemistry for Iba1 in the lumbar part of the spinal cord of wild-type (A) and *Mrs2*^{dmy}/*Mrs2*^{dmy} rats (B) at 6 weeks of age. Signals of Iba1 (AlexaFluor 546 nm; red), which is upregulated during the activation of microglia, are seen in *Mrs2*^{dmy}/*Mrs2*^{dmy} rats much more the wild-type control. Nucleus is stained with DAPI (blue). C, Inflammatory cytokine mRNA expression in the CNS of wild-type (□) and *Mrs2*^{dmy}/*Mrs2*^{dmy} (■) rats. IL1b expression was elevated in *Mrs2*^{dmy}/*Mrs2*^{dmy} rats at 4 and 6 weeks of age. IL6 was elevated in *Mrs2*^{dmy}/*Mrs2*^{dmy} rats at 6 weeks of age. * $P<0.05$, ** $P<0.005$.
doi:10.1371/journal.pgen.1001262.g005

initial development of myelin (myelination) are different from those that are involved in its maintenance and turnover since, in *Mrs2*^{dmy}/*Mrs2*^{dmy} rats, myelin development is normal while its maintenance is defective. Our mutant rats also appear to be an excellent animal model, not only to evaluate the causal relationships between primary mitochondrial dysfunction and subsequent demyelination, but also for the development of therapies making use, for example, of cell transplantation.

Materials and Methods

Genetic fine mapping of *dmy*

Congenic strains WTC (NBRP#0020) and WTC.DMY-*dmy* (NBRP#0021) were both from the National BioResource Project - Rat, Kyoto University (Kyoto, Japan). (WTC.DMY-*dmy* × BN/SsNSlc)F1(+/*dmy*) rats were intercrossed to produce F2 progeny. *dmy*/*dmy* homozygotes were identified at 7–8 weeks of age, when paralysis of the hind limbs was obvious. 687 *dmy*/*dmy* rats were collected out of 3,252 F2 animals (~21%) and used for fine mapping of the *dmy* locus. Simple sequence length polymorphisms (SSLPs) from the *Prl* (prolactin) and *Hh1tts* (Testis-specific histone, H1t and H4t) genes were used for genotyping as described [31]. To refine the limits of the recombinant interval between *Prl* and *Hh1tts*, two gene-specific and one anonymous SSLP markers were used: *Mrs2* (5′-TCTCCCTTGCCTCTATCTCTCGTCT-3′,5′-CCTGCAGTACTGGGTAAGCCTGATG-3′), *Aldh5a1* (5′-GTTAACTGCACAAGAGCAAGCCAGT-3′, 5′-GCTAATGTTAAGTCATGGGGTGAGG-3′), and *D17Kur17* 5′-ACCTCTTTTTGCCAGCATTG-3′, 5′-CCCTGGGATTGGTCCATA-3′).

All animal experiments were approved by the Animal Research Committee of Kyoto University and were conducted according to the Regulations on Animal Experimentation of Kyoto University.

RT-PCR and direct sequencing

Total RNA was isolated from the brain of 5-week-old animals using ISOGEN (NIPPON GENE, Tokyo, Japan). RT-PCR and direct sequencing of the PCR products were carried out as described previously [32].

Transgenic rescue and recombinant BAC transgenics

A construct containing the CMV promoter, 1.45-kb of the *Mrs2* coding sequence, and SV40 polyA signal was excised from the vector (pCMV-Script; Agilent Technologies, CA, USA) and used as a transgene, which was microinjected into the pronuclei of fertilized oocytes collected from Crj:Wistar rats. Transgenic offspring founder rats were then crossed with WTC- +/*dmy* rats and then backcrossed again to WTC- +/*dmy* rats to obtain *dmy*/*dmy* homozygous and also hemizygous for the transgene (*dmy*/*dmy*, tg/-). Expression of the transgene was confirmed by RT-PCR with primers (5′-GCGAATGGAGATCCAATTTT-3′, 5′-GGGAGGTGTGGGAGGTTTT-3′) to detect SV40 polyA sequence. Brain RNA was treated with DNase I (New England BioLabs) to remove contaminating genomic DNA and then subjected to cDNA synthesis.

A rat BAC clone, CHORI-230-9K13, including the rat *Mrs2* gene was modified to express MR2SL-EGFP fusion protein under the endogenous promoter by ET recombination technology [33]. Modified genomic DNA was excised from the vector and then used for *in ovo* transgenesis.

Quantitative PCR

Real-time PCR was performed using the Thermal Cycler Dice Real Time System (Takara Bio Inc., Otsu, Japan) with SYBR Premix Ex Taq II (Takara Bio Inc., Otsu, Japan). By monitoring amplification curves of a test sample and reference samples that contained 101–106 molecules of the gene of interest, the number of target molecules in the test sample was analyzed. The number of target molecules was normalized to that of glyceraldehyde-3-phosphate dehydrogenase (*Gapdh*) as an internal control. The primers used are as follows: 5′-GCTGTGGCAGCTACCTATGTCTTG-3′ and 5′-AGGTCGTCATCATCCCACGAG-3′ for the rat Interleukin-1b (*Il1b*), 5′-CCACTTCACAAGTCGGAGGCTTA-3′ and 5′-GTGCATCATCGCTGTTCATACAATC-3′ for the rat interleukin-6 (*Il6*), 5′-GGCACAGTCAAGGCTGAGAATG-3′ and 5′-ATGGTGGTGAAGACGGCCAGTA-3′ for rat *Gapdh*.

Electron microscopy

Perfusion fixation through the left ventricle was conducted with 4% paraformaldehyde in 0.1 M phosphate buffer (PB). Brains and spinal cords were dissected and stored in 2% paraformaldehyde and 2.5% glutaraldehyde in 0.1 M PB, then post-fixed with 2% osmic acid for 2 hours and embedded in epoxy resin. Ultrathin sections were double-stained with uranyl acetate and lead citrate and examined by a Hitachi H-7500 electron microscope (Hitachi, Tokyo, Japan).

Immunohistochemistry

Immunohistochemistry was performed as described previously [9]. The following primary antibodies were used: monoclonal anti-2′, 3′-cyclic nucleotide-3′-phosphodiesterase (CNPase) for oligodendrocytes (1:1,000; Sigma, St. Louis, MO, USA), monoclonal anti-mitochondria (1:100; Abcam, Cambridge, MA, USA), polyclonal anti-GFAP for astrocytes (1:1,000; Dako, Carpinteria, CA, USA), polyclonal anti-Iba1 for microglia/macrophages (1:200; Wako Pure Chemical Industries, Osaka, Japan). Cy3-conjugated anti-mouse IgG (1:500; Jackson Laboratories) or Alexa 588-conjugated anti-rabbit IgG (1:500; Molecular Probes) antibody was reacted. Nuclei were counterstained with DAPI (Vactor Laboratories). Signals were detected with a fluorescence microscopy (Olympus, Tokyo, Japan) or a confocal imaging system (C1Si; Nikon, Tokyo, Japan).

For immunoelectron microscopy, PFA-perfused frozen sections were incubated with rabbit antibody against fluorescent protein (1:2,000; Molecular Probes) at 4 °C overnight. After washing in PBS, peroxidase-conjugated anti-rabbit IgG Fab fraction (Jackson Laboratories, 1:1,000) and immunoreactions were reacted 3,3-diaminobenzidine substrate kit (Vector Laboratories), postfixed in 1% osmium tetraoxide, dehydrated in graded ethanol, and then embedded in epoxy resin. Ultrathin sections were examined by electron microscopy (Hitachi, Tokyo, Japan).

Lactic acid measurements

Cerebrospinal fluid was collected from *dmy*/*dmy*, wild-type littermates, and *dmy*/*dmy* with the normal *Mrs2* transgene at 6–7 weeks of age under isoflurane anesthesia. They were then mixed with 0.8N perchloric acid to inactivate proteins. After centrifugation, lactic acid concentrations of the supernatants were measured by Determiner LA (KYOWA MEDEX Co., Ltd., Tokyo, Japan).

Cytochrome oxidase histochemistry

Frozen spinal cord sections were prepared. Then, 100 µl of freshly prepared reaction buffer [50 mM Tris/HCl (pH 7.4), 0.5 mg/ml diaminobenzidine, 20 µg/ml catalase and 0.50 mg/ml cytochrome C] was added to each section and slides were incubated for 30 min at 37°C.

ATP measurements

Rats were sacrificed by cervical dislocation and the brains were immediately excised, frozen in liquid nitrogen, and stored at −80°C until measurement. In order to release cellular ATP, frozen tissue (25 mg) was boiled for 2 min after the addition of 300 µl water containing 100 mM Tris/HCl (pH 7.75) and 4 mM EDTA. Samples were placed on ice and homogenized by sonification (micro tip, 1 s ×10 pulse). ATP concentrations were determined using the ATP bioluminescence assay kit HS II (Roche) according to the manufacturer's protocol. Data were standardized to the protein concentration which was determined by Coomassie Plus – the better Bradford assay kit (Pierce).

Statistical analysis

Statistical differences in lactic acid, ATP and mRNA expressions between wild-type and *dmy*/*dmy* rats were evaluated using the Mann-Whitney U test.

Supporting Information

Figure S1 Detection of the $Mrs2^{dmy}$ mutation. A. Chromatograms showing the $Mrs2^{dmy}$ G-to-A mutation. Upper: wild-type genome. Lower: $Mrs2^{dmy}/Mrs2^{dmy}$ genome. The $Mrs2^{dmy}$ mutation disrupted *Act*I restriction site (GGCG) in the $Mrs2^{dmy}/Mrs2^{dmy}$ genome. B. Molecular diagnosis of the $Mrs2^{dmy}$ mutation. In the wild type, the 349-bp PCR product amplified with primers rMrs2-31&32 (5′-AAAGTTTGACAAAGAAGGAAACG-3′ and 5′-GGGGATGGAGGGCTATGTAA-3′) is digested with *Act*I but not in $Mrs2^{dmy}/Mrs2^{dmy}$ mutant rats. M: ΦX174-*Hae*III digests.
Found at: doi:10.1371/journal.pgen.1001262.s001 (1.15 MB TIF)

Figure S2 Transgenic rescue experiment. A. Expression of the transgene in the brain of a transgenic rat. Brain cDNA from Tg-

positive rats (Lanes 2 and 3) and Tg-negetive rats (Lanes 1and 4) was used as templates. Brain RNA was treated with DNaseI to remove contaminating genomic DNA. M: ΦX174 *Hae*III digests. B. Histopathology of the cervical part of the spinal cord of *dmy/dmy* transgene-negative rats (left) and *dmy/dmy* transgene-positive (right) rats aged 10 weeks. Luxol fast blue-HE staining. Original magnification: ×100. C. Lactic acid concentration in cerebrospinal fluid of 6-7-week-old *dmy/dmy* rats and age-matched *dmy/dmy Mrs2* cDNA-transgenic rats. Elevated lactic acid (126 ± 43.7 mg/dL) was reduced to normal level (22 ± 3.1 mg/dL). **, $P < 0.002$. D. Electron microphotograph of an oligodendrocyte in a *dmy/dmy* transgene-positive rat. Densely packed mitochondria (arrowheads) were found in the cytoplasm. Bar: 2μm.
Found at: doi:10.1371/journal.pgen.1001262.s002 (5.52 MB TIF)

Figure S3 MRS2 expression in the CNS of Mrs2-GFP recombinant BAC transgenic rats. MRS2 signals were mainly found in neurons (A), and occasionally in GFAP-positive astrocytes (B) and CNP-positive oligodendrocytes (C). Left: Bar: 50 μm. Center, Right: Bar: 20 μm.
Found at: doi:10.1371/journal.pgen.1001262.s003 (3.15 MB TIF)

Figure S4 MRS2 expression in Mrs2-GFP recombinant BAC transgenic rats. MRS2 signals were observed in the myocardium (A), liver (B), testis (C) and skeletal muscles (D). Bar: 50 μm.
Found at: doi:10.1371/journal.pgen.1001262.s004 (6.29 MB TIF)

Figure S5 Sequence alignment of yeast, human, and rat MRS2 proteins. Predicted transmembrane domains (TM-1, TM-2) are boxed; * indicates identical residues; : indicates conservative substitution; . indicates semiconservative substitutions. The sequence of a motif conserved in all putative magnesium transporters, G-M-N, is indicated in bold. Predicted coiled-coil regions are underlined, five regions with conserved amino acid residues (CRB-1-5; conserved residue block) are shaded grey. Arrowhead: The position of the residue affected by the *dmy* mutation, after which the 15 additional residues follow in mutant MRS2.
Found at: doi:10.1371/journal.pgen.1001262.s005 (1.38 MB TIF)

Acknowledgments

The authors are grateful to M. Yokoe for excellent technical assistance.

Author Contributions

Conceived and designed the experiments: TK. Performed the experiments: TK MK ST TI YN KK. Analyzed the data: TK MK. Contributed reagents/materials/analysis tools: MA TS. Wrote the paper: TK MK JLG.

References

1. Werner H, Jung M, Klugmann M, Sereda M, Griffiths IR, et al. (1998) Mouse models of myelin diseases. Brain Pathol 8: 771–793.
2. Griffiths IR (1996) Myelin mutants: model systems for the study of normal and abnormal myelination. Bioessays 18: 789–797.
3. Meyer Zu Horste G, Nave KA (2006) Animal models of inherited neuropathies. Curr Opin Neurol 19: 464–473.
4. Kuramoto T, Sotelo C, Yokoi N, Serikawa T, Gonalons Sintes E, et al. (1996) A rat mutation producing demyelination (*dmy*) maps to chromosome 17. Mamm Genome 7: 890–894.
5. Kitada K, Guenet JL, Serikawa T (2000) Determination of the mouse homologous region for the rat *dmy* locus. J Exp Anim Sci 41: 40–43.
6. Schindl R, Weghuber J, Romanin C, Schweyen RJ (2007) Mrs2p forms a high conductance Mg^{2+} selective channel in mitochondria. Biophys J 93: 3872–3883.
7. Gregan J, Bui DM, Pillich R, Fink M, Zsurka G, et al. (2001) The mitochondrial inner membrane protein Lpe10p, a homologue of Mrs2p, is essential for magnesium homeostasis and group II intron splicing in yeast. Mol Gen Genet 264: 773–781.
8. Schock I, Gregan J, Steinhauser S, Schweyen R, Brennicke A, et al. (2000) A member of a novel Arabidopsis thaliana gene family of candidate Mg^{2+} ion transporters complements a yeast mitochondrial group II intron-splicing mutant. Plant J 24: 489–501.
9. Kuwamura M, Kanehara T, Tokuda S, Kumagai D, Yamate J, et al. (2004) Immunohistochemical and morphometrical studies on myelin breakdown in the demyelination (*dmy*) mutant rat. Brain Res 1022: 110–116.
10. Kolisek M, Zsurka G, Samaj J, Weghuber J, Schweyen RJ, et al. (2003) Mrs2p is an essential component of the major electrophoretic Mg^{2+} influx system in mitochondria. Embo J 22: 1235–1244.
11. Piskacek M, Zotova L, Zsurka G, Schweyen RJ (2009) Conditional knockdown of hMRS2 results in loss of mitochondrial Mg^{2+} uptake and cell death. J Cell Mol Med 13: 693–700.
12. Wiesenberger G, Waldherr M, Schweyen RJ (1992) The nuclear gene MRS2 is essential for the excision of group II introns from yeast mitochondrial transcripts in vivo. J Biol Chem 267: 6963–6969.
13. Devivo DC (1993) The expanding clinical spectrum of mitochondrial diseases. Brain Dev 15: 1–22.
14. Huttemann M, Zhang Z, Mullins C, Bessert D, Lee I, et al. (2009) Different proteolipid protein mutants exhibit unique metabolic defects. ASN Neuro 1.
15. Thambisetty M, Newman NJ (2004) Diagnosis and management of MELAS. Expert Rev Mol Diagn 4: 631–644.
16. Bui DM, Gregan J, Jarosch E, Ragnini A, Schweyen RJ (1999) The bacterial magnesium transporter CorA can functionally substitute for its putative homologue Mrs2p in the yeast inner mitochondrial membrane. J Biol Chem 274: 20438–20443.
17. Zsurka G, Gregan J, Schweyen RJ (2001) The human mitochondrial Mrs2 protein functionally substitutes for its yeast homologue, a candidate magnesium transporter. Genomics 72: 158–168.
18. Eshaghi S, Niegowski D, Kohl A, Martinez Molina D, Lesley SA, et al. (2006) Crystal structure of a divalent metal ion transporter CorA at 2.9 angstrom resolution. Science 313: 354–357.
19. Detmer SA, Chan DC (2007) Functions and dysfunctions of mitochondrial dynamics. Nat Rev Mol Cell Biol 8: 870–879.
20. Hung PC, Wang HS (2007) A previously undescribed leukodystrophy in Leigh syndrome associated with T9176C mutation of the mitochondrial ATPase 6 gene. Dev Med Child Neurol 49: 65–67.
21. Navarro-Sastre A, Martin-Hernandez E, Campos Y, Quintana E, Medina E, et al. (2008) Lethal hepatopathy and leukodystrophy caused by a novel mutation in MPV17 gene: description of an alternative MPV17 spliced form. Mol Genet Metab 94: 234–239.
22. Spinazzola A, Viscomi C, Fernandez-Vizarra E, Carrara F, D'Adamo P, et al. (2006) MPV17 encodes an inner mitochondrial membrane protein and is mutated in infantile hepatic mitochondrial DNA depletion. Nat Genet 38: 570–575.
23. Zafeiriou DI, Koletzko B, Mueller-Felber W, Paetzke I, Kueffer G, et al. (1995) Deficiency in complex IV (cytochrome c oxidase) of the respiratory chain, presenting as a leukodystrophy in two siblings with Leigh syndrome. Brain Dev 17: 117–121.
24. Andrews HE, Nichols PP, Bates D, Turnbull DM (2005) Mitochondrial dysfunction plays a key role in progressive axonal loss in Multiple Sclerosis. Med Hypotheses 64: 669–677.
25. Mahad DJ, Ziabreva I, Campbell G, Lax N, White K, et al. (2009) Mitochondrial changes within axons in multiple sclerosis. Brain 132: 1161–1174.
26. Lopez MF, Kristal BS, Chernokalskaya E, Lazarev A, Shestopalov AI, et al. (2000) High-throughput profiling of the mitochondrial proteome using affinity fractionation and automation. Electrophoresis 21: 3427–3440.
27. Pagliarini DJ, Calvo SE, Chang B, Sheth SA, Vafai SB, et al. (2008) A mitochondrial protein compendium elucidates complex I disease biology. Cell 134: 112–123.
28. Dheen ST, Kaur C, Ling EA (2007) Microglial activation and its implications in the brain diseases. Curr Med Chem 14: 1189–1197.
29. Merrill JE, Scolding NJ (1999) Mechanisms of damage to myelin and oligodendrocytes and their relevance to disease. Neuropathol Appl Neurobiol 25: 435–458.
30. Mitrovic B, Ignarro LJ, Montestruque S, Smoll A, Merrill JE (1994) Nitric oxide as a potential pathological mechanism in demyelination: Its differential effects on primary glial cells in vitro. Neuroscience 61: 575–585.
31. Serikawa T, Kuramoto T, Hilbert P, Mori M, Yamada J, et al. (1992) Rat gene mapping using PCR-analyzed microsatellites. Genetics 131: 701–721.
32. Kuramoto T, Kitada K, Inui T, Sasaki Y, Ito K, et al. (2001) Attractin/mahogany/zitter plays a critical role in myelination of the central nervous system. Proc Natl Acad Sci U S A 98: 559–564.
33. Zhang Y, Buchholz F, Muyrers JP, Stewart AF (1998) A new logic for DNA engineering using recombination in *Escherichia coli*. Nat Genet 20: 123–128.

Kuramoto et al. BMC Genetics 2011, 12:91
http://www.biomedcentral.com/1471-2156/12/91

BMC Genetics

RESEARCH ARTICLE Open Access

A rat model of hypohidrotic ectodermal dysplasia carries a missense mutation in the *Edaradd* gene

Takashi Kuramoto*, Mayuko Yokoe, Ryoko Hashimoto, Hiroshi Hiai and Tadao Serikawa

Abstract

Background: Hypohidrotic ectodermal dysplasia (HED) is a congenital disorder characterized by sparse hair, oligodontia, and inability to sweat. It is caused by mutations in any of three Eda pathway genes: ectodysplasin (*Eda*), Eda receptor (*Edar*), and Edar-associated death domain (*Edaradd*), which encode ligand, receptor, and intracellular adaptor molecule, respectively. The Eda signaling pathway activates NF-κB, which is central to ectodermal differentiation. Although the causative genes and the molecular pathway affecting HED have been identified, no curative treatment for HED has been established. Previously, we found a rat spontaneous mutation that caused defects in hair follicles and named it sparse-and-wavy (*swh*). Here, we have established the *swh* rat as the first rat model of HED and successfully identified the *swh* mutation.

Results: The *swh/swh* rat showed sparse hair, abnormal morphology of teeth, and absence of sweat glands. The ectoderm-derived glands, meibomian, preputial, and tongue glands, were absent. We mapped the *swh* mutation to the most telomeric part of rat Chr 7 and found a Pro153Ser missense mutation in the *Edaradd* gene. This mutation was located in the death domain of EDARADD, which is crucial for signal transduction and resulted in failure to activate NF-κB.

Conclusions: These findings suggest that *swh* is a loss-of-function mutation in the rat *Edaradd* and indicate that the *swh/swh* rat would be an excellent animal model of HED that could be used to investigate the pathological basis of the disease and the development of new therapies.

Background

Hypohidrotic ectodermal dysplasia (HED) is a genetic disorder characterized by sparse hair, oligodontia, reduced sweating, and defects in a number of other ectodermal organs [1]. A lack of sweat glands can lead to recurrent severe overheating. Thus, children with HED are at substantial risk of sudden death in infancy due to fatal hyperpyrexia [2].

HED is caused by mutations in any of the three Eda pathway genes: ectodysplasin (*Eda*) [3,4], ED receptor (*Edar*) [5], and EDAR-associated death domain (*Edaradd*) [6]. They encode the ligand, receptor, and intracellular signal mediator of a single linear pathway, respectively. The Eda signaling pathway activates transcription factor NF-κB thereby playing an important role in embryonic development, especially in the development of ectodermally derived organs [1].

In humans, there are three types of HED with different inheritance: X-linked HED, autosomal dominant HED, and autosomal recessive HED. X-linked HED is the most common form of HED and is caused by mutations in *EDA*. Autosomal HED is caused by mutations in *EDAR* or *EDARADD*. Currently, over 100 different mutations in the *EDA* gene are known, while only ~20 and 4 causative mutations have been found in *EDAR* and *EDARADD*, respectively [7].

To date, four mouse models of HED are available: *Tabby, downless, Sleek*, and *crinkled*. The mutant phenotype of the *Tabby* mouse is inherited in an X-linked manner and the *Tabby* mouse carries a mutation in the *Eda* gene [4]. The recessive *downless* and dominant *Sleek* mice carry mutations in the *Edar* gene [8]. The *crinkled* mouse carries a mutation in the *Edaradd* gene [6]. The phenotypes in *Eda, Edar*, and *Edaradd* mutant mice are almost identical and include abnormalities in teeth, hair, and sweat glands, the triad of symptoms of HED. Over 20 different glands, including lacrimal, meibomian, salivary,

* Correspondence: tkuramot@anim.med.kyoto-u.ac.jp
Institute of Laboratory Animals, Graduate School of Medicine, Kyoto University, Yoshidakonoe-cho, Sakyo-ku, Kyoto 606-8501, Japan

submandibular, and mammary glands, are also affected [9-11]. These mutant mice have been used to study the roles of the Eda pathway in the development and morphogenesis of ectoderm-derived organs and to develop a novel treatment for HED using a recombinant EDA protein [12].

Mutations in some of the genes in the Eda pathway have been identified in various species, such as medaka [13], zebrafish [14], cattle [15-18], and dog [19]. Analyses of these mutations showed critical roles of the Eda pathway in the development of epithelial appendages, as well as in morphological evolution. Thus, the identification of novel mutations in different species emphasized the importance of the Eda pathway, and enabled the phenotypes of the mutated animals to be compared, giving new insights into the functions of the Eda pathway. If such novel mutations can be identified in mammals, then the affected species could be used as a disease model of HED.

In a previous study, we described a mutant rat, sparse and wavy hair (*swh*), which arose spontaneously in a colony of inbred WTC rats in 1998 [20]. The mutant phenotype is characterized by sparse and wavy hair, impaired body weight gain, and hypoplasticity of the mammary gland. The hair follicles in these rats were reduced both in number and size, a characteristic associated with hypoplasia of both the sebaceous glands and the subcutaneous fat tissues. The mammary glands of *swh/swh* female rats were hypoplastic and differentiation of mammary epithelial and myoepithelial cells was impaired. Thus, it is conceivable that the *swh/swh* rat will provide a good experimental model to clarify the mechanisms involved in the development of skin appendages, most of which are derived from ectoderm [20].

In our previously reported linkage analysis, *swh* mapped to the telomeric part of rat Chr 17. At that time, the physical location of the *swh* locus could not be accurately determined because a SSLP marker, *D17Rat140*, which defined the distal side of the *swh* locus was, in the earlier public rat genome linkage map, erroneously assigned to the middle part of Chr 17 and not to the telomeric part of Chr 17. Recently, with the development of more than 20,000 single nucleotide polymorphism (SNP) markers for 167 rat inbred strains and with the haplotype mapping data from the genotyping of these SNPs, the genome linkage map has been improved [21]. In the improved rat genome map, *D17Rat140* and its neighboring genes are correctly mapped to the telomeric part of rat Chr 17. Thus, in addition to the 24 candidate genes selected from our previous linkage analysis, we also considered these newly mapped genes to be candidates of *swh* [20].

In this study, to demonstrate the suitability of the *swh* rat as an HED model, we investigated the pathology of tissues and organs in which morphological abnormalities in HED are known to occur. Furthermore, we identified the causative mutation of the *swh* phenotype using a positional cloning approach, and found a missense mutation in the death domain of EDARADD, that might explain the inability of the mutant *Edaradd* gene to activate NF-κB. Our findings suggest that *swh* is a loss-of-function mutation of the rat *Edaradd* and support the *swh/swh* rat as an excellent animal model of HED that can be used to investigate the pathological basis of the disease and to develop new therapies.

Methods

Animals

ACI/NKyo, WTC/Kyo, and WTC-*swh*/Kyo rats were provided by the Japanese National BioResource Project for the Rat and kept in our animal facility for all experiments in this study. Animal care and experimental procedures were approved by the Animal Research Committee, Kyoto University, Japan, and were conducted according to the Regulation on Animal Experimentation at Kyoto University.

Histopathology

For light microscopy, the tongue, eyelid, ventral skin, footpad, and preputial gland were harvested from WTC-*swh/swh* and WTC rats at 8 weeks of age. Tissues were fixed in 10% neutral-buffered formalin, embedded in paraffin, and stained with hematoxylin and eosin (HE).

Sweat tests and whole mount staining of mammary glands

The sweat test was performed as described previously [12]. Briefly, the hind paws of rats anesthetized with sevoflurane were painted with a solution of 3% (wt/vol) iodine in ethanol. Once dry, the paws were painted with a suspension of 40% (wt/vol) starch I mineral oil. Photographs were taken 1 min later and sweat was detected as dark spots. Mammary glands were prepared as a whole mount and stained as described previously [22].

Fine mapping of swh

For fine mapping of *swh*, F2 animals (n = 769) were produced by intercrossing (ACI/NKyo × WTC-*swh*) F1 rats. Homozygous *swh/swh* animals were identified at 3-4 weeks of age based on the appearance of the sparse-and-waved hair phenotype. One hundred and ninety-eight *swh/swh* homozygotes were used for fine mapping of *swh*. Genomic DNA was prepared from tail biopsies using the automatic DNA purification system (PI-200; Kurabo, Japan).

RNA extraction, RT-PCR and direct sequencing

Total RNA was extracted from the skin of 2-week-old animals. RNA preparation, RT-PCR and direct sequencing of PCR products were performed as described

previously [23]. Rat *Edaradd* cDNAs were amplified with 6 sets of primers (Table 1). The PCR products overlapped each other and spanned the entire coding sequence of *Edaradd*.

Transient transfection and reporter assays

The NF-κB assay was designed to test for activation of the NF-κB responsive promoter. HEK293T cells grown in poly-L-lysine coated 24-well plates were transfected using SuperFect (Qiagen) with 1.2 μg pNF-κB-Luc (Clontech), 2 μg pRL-TK, and an increasing amount of expression vectors encoding the wild-type EDARADD or the *swh*-type EDARADD (Pro153Ser). The Luc reporter of the pNF-κB-Luc encodes firefly luciferase. The HSV-TK (herpes simplex virus thymidine kinase) promoter drives renilla luciferase in pRL-TK. Total DNA was adjusted to 2.6 μg by adding pCMV-HA (Clontech) vector as necessary. Luciferase activity was measured using the Dual-Luciferase Reporter Assay System (Promega) 48 h after transfection, according to the manufacturer's protocol.

Results

Phenotypes of *swh/swh* rat as hypohidrotic ectodermal dysplasia (HED)

Patients with HED display defective development of hair, teeth, sweat glands, and several exocrine glands, such as sebaceous, salivary, meibomian, and lacrimal [1,24]. To evaluate the relevance of the *swh/swh* rat as a HED model, we looked for developmental defects in those tissues of *swh/swh* rats. In addition to defects of the hair, skin, and mammary glands, which have been reported previously [20] (Figure 1A, B), we found defects in the sweat, meibomian, preputial, and tongue glands. In these tissues, the exocrine glands were absent in the *swh/swh* rats (Figure 1C, D, E, F). In the sweat test, no sweat was detected in *swh/swh* rats, indicating that the sweat glands were functionally defective (Figure 1C). We also found a reduced number of cusps in the lower first molars in the *swh/swh* rats (Figure 1G).

In the Eda pathway mutant mice, *Tabby, downless*, and *crinkled*, a kinked tail tip, a bald patch behind the ear, and abnormal pelage hair composition are characteristic. Similarly, in *swh/swh* rat, the pelage hair was composed of only an abnormal awl hair (Figure 1A); however, the tail had hair on it, the frequency of kinked tail was low, and the bald patch behind the ear was not found (Figure 1G).

These findings indicate that the mutant phenotypes of *swh/swh* rats are similar to developmental defects in HED patients and in the established mouse models; therefore, it is likely that the *swh/swh* rat will be suitable as a model of HED.

Positional cloning of *swh*

In a previous study, we mapped *swh* to rat Chr 17 [20]. To more specifically map the position of the *swh* locus, we genotyped F2 intercross progeny for markers known to be closely linked to *swh*. There was only one recombinant chromosome between *swh* and either *D17Rat132* or *D17Rat140* in 396 meioses (= 198 × 2) and we were able to map *swh* to the most distal part of Chr17 (Figure 2A). The rat genome map (RGSC v3.4) showed two genes in the *swh* locus, *Ero1lb* (ERO1-like beta (*S. cerevisiae*)) and *Edaradd* (ectodysplasin-A receptor-associated death domain). The mouse mutant of *Edaradd* is called *crinkled* (*cr*) and mice that carry this mutation show a sparse hair phenotype that is similar to that of the *swh* rat [25]. Additionally, mutations in the human *EDARADD* gene have been found in families affected with HED [6,26]. Thus, we considered *Edaradd* as a good candidate of *swh*. Although the abnormal expression of *Edaradd* mRNA was not detected in the skin of *swh/swh* rats (data not shown), we found a missense mutation (C to T) in exon 6 of the *swh/swh Edaradd* gene. This mutation was deduced to change proline to serine at the 153rd amino acid (Pro153Ser) of the rat EDARADD protein (Figure 2B). The 153rd amino acid is located in the death domain of EDARADD and is highly conserved in vertebrates (Figure 2C). These findings suggest that the Pro153Ser missense mutation of the *Edaradd* gene is causative of the phenotypes of *swh/swh* rats.

Reporter assay for the Pro153Ser mutant EDARADD

Overexpression of *Edaradd* in 293T cells activates NF-κB in a dose-dependent manner [25]. To examine whether Pro153Ser *Edaradd* can activate NF-κB, we carried out a reporter assay. As shown in Figure 3, wild-type *Edaradd*

Table 1 PCR primers used to amplify rat *Edaradd* cDNA

Primer set	Forward (5' > 3')	Reverse (5' > 3')
Edaradd-1&2	CTGAGAGAGAGTCGCGCATT	GCCACAGCTGTTCCCATAG
Edaradd-3&4	GCCCAGAAAAGGCAGCTC	GGAAAACCTTTGGAGTTTCTGA
Edaradd-5&6	CGATGAGCCAGCTTTACCTC	GGATAATTGGGTAACTATTCTCAACC
Edaradd-7&8	TCCATCCCAATTTTACCAACA	CGGCAAGCATTTTAATGACC
Edaradd-9&10	CAGTCAGCCCCTTGCACT	GCATGCTCTCATCAACATGG
Edaradd-11&12	TGTCACCAATGTGGTAGAAAAA	CAGGGATAACCACTGCCTGT

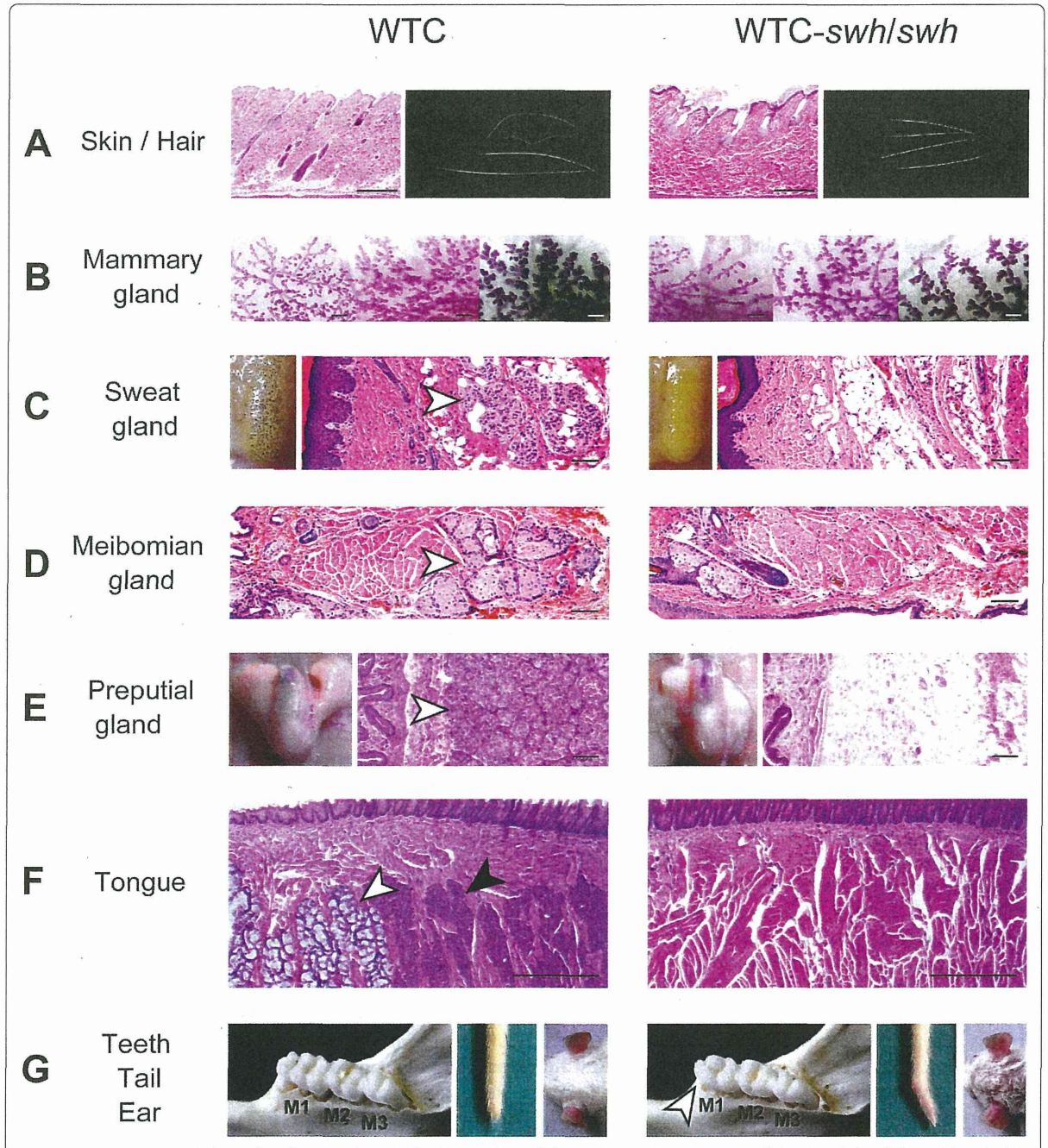

Figure 1 Phenotypes of the swh/swh rat as hypohidrotic ectodermal dysplasia (HED). A, Sections of the dorsal skin (left) and hair (right). Incomplete hair follicles are evident in *swh/swh* rat. Scale bar, 0.5 mm. The WTC rat has four hair types; auchene, zigzag, awl and guard, while the *swh/swh* rat have only the abnormal awl hair. B, Whole mount stained mammary glands; 6-week-old (left), 8-week-old (center), and pregnant day 9 (right). Mammary gland branching is poor in *swh/swh* rat. Scale bar, 1 mm. C, Sweat test results (left) and section of the footpads. Sweat, detected as dark spots, is not seen in *swh/swh* rat. Sweat glands (arrowhead) are present in WTC rat and absent in *swh/swh* rat. Scale bar, 100 μm. D, Sections of the eyelid. The meibomian glands (arrowhead) are present in WTC rat and absent in *swh/swh* rat. Scale bar, 100 μm. E, An entire view (left) and a section of the preputial gland (right). The preputial gland is atrophied in male *swh/swh* rat. Acinous glands (arrowhead) are present in WTC rat and absent in *swh/swh* rat. Scale bar, 100 μm. F, Section of the tongue. Both mucous (open arrowhead) and serous (filled arrowhead) glands are present in WTC rat and neither is seen in *swh/swh* rat. Scale bar, 0.5 mm. **G**, Buccal views of lower molars (left), tip of tail (center), and posterior auricular region (right). Cusp number is reduced in the first molar (arrow head) in *swh/swh* rat. Some *swh/swh* rats show the kink tail. The bald patch behind the ear was not evident in the *swh/swh* rat.

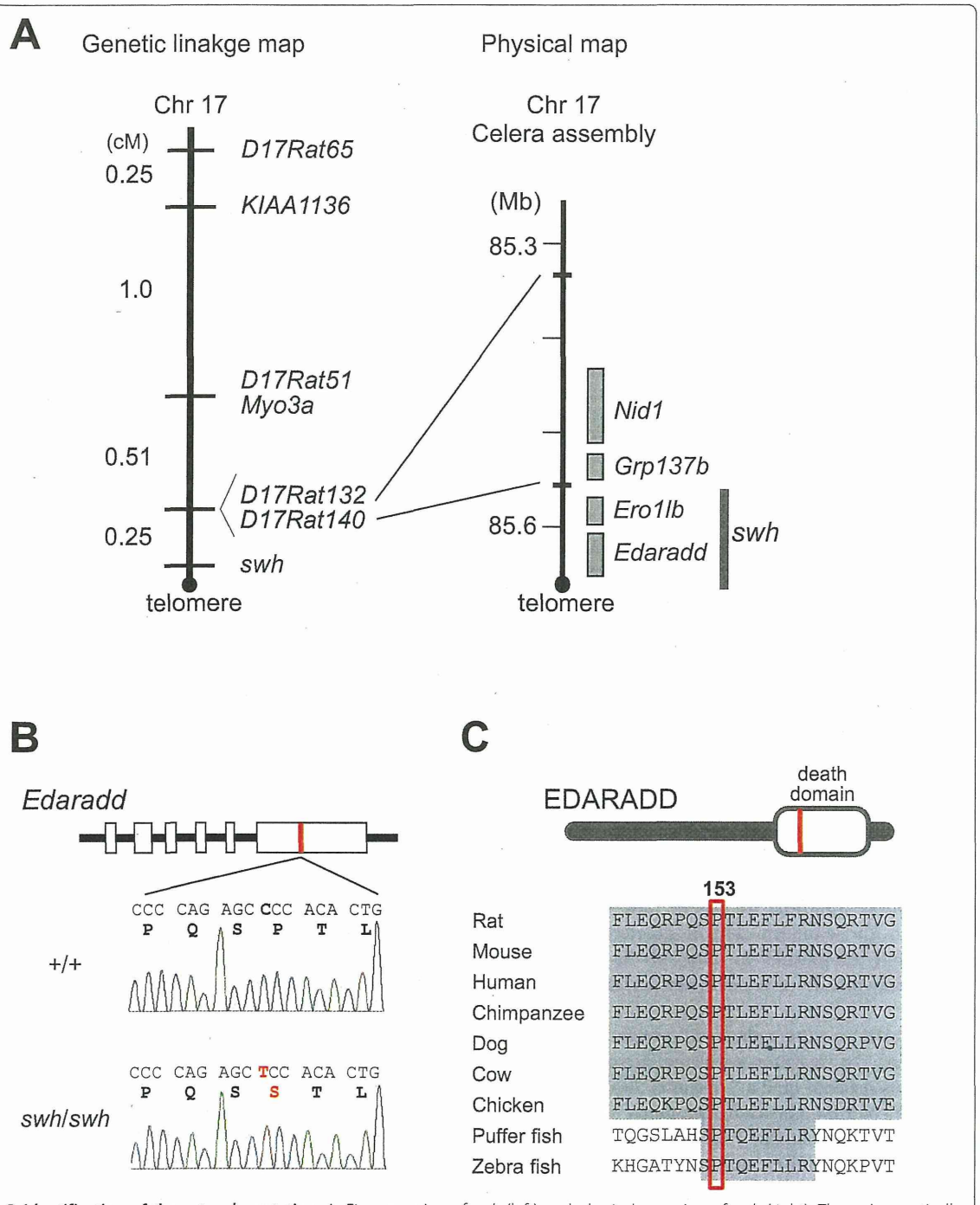

Figure 2 Identification of the rat *swh* mutation. A, Fine mapping of *swh* (left) and physical mapping of *swh* (right). The *swh* genetically mapped to the most telomeric part of rat Chr17, 0.25-cM distal from *D17Rat132* and *D17Rat140*. In the physical map, the *swh* locus is localized to a ~0.2-Mb region between *D17Rat140* and the telomere. Both *Ero1lb* and *Edaradd* have been mapped within the *swh* locus. B, Sequence analysis of *Edaradd* gene of wild-type and *swh/swh* rats. In the genomic DNA of *swh/swh* rat, a C to T (red) transition is present in exon 6 of rat *Edaradd* gene. This changes proline to serine at codon 153 of the deduced EDARADD protein. Rat codon 153 corresponds to codon 156 of mouse EDARADD isoform 1 (NP_598398) and codon 153 human EDARADD isoform B (NP_542776). C, Amino-acid sequence alignment of a region of the EDARADD death domain from different species. The 153rd amino acid that is altered in *swh/swh* rat is highly conserved in the vertebrates.

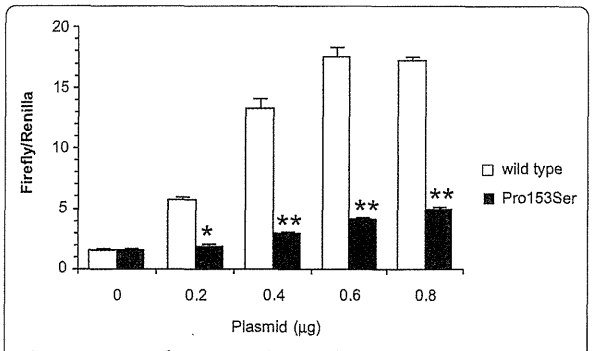

Figure 3 Loss of NF-κB activation by the Pro153Ser Edaradd mutant protein. 293T cells were transfected with 1.2 μg pNF-κB-luciferase reporter gene plasmid, 2 μg pRL-TK, and the amounts of each expression construct were measured in a reporter assay. The expression levels of luciferase were normalized to those of the internal control. Relative NF-κB activity in wild-type transfected cells increased in a dose-dependent manner, while significantly lower relative NF-κB activity was observed in the Pro153Ser *Edaradd*-transfected cells. *P < 0.01, **P < 0.001.

activated NF-κB in a dose-dependent manner. Meanwhile, Pro153Ser *Edaradd* showed significantly lower transcriptional activity of NF-κB than the wild type. The expression level of the Pro153Ser EDARADD protein detected by western blotting was not different from that of the wild type (data not shown). These findings indicate that the Pro153Ser missense mutation of the rat *Edaradd* gene could not activate NF-κB and that the Eda signaling pathway failed to function in *swh/swh* rats.

Discussion

In this study, we demonstrated that the *swh/swh* rat harbored a Pro153Ser mutation in the *Edaradd* gene and showed typical symptoms of HED, such as sparse hair, oligodontia, inability to sweat, and developmental defects of the ectoderm-derived glands [27]. Hence, we successfully established the *swh/swh* rat as a genetically and phenotypically well-characterized disease model of HED.

EDARADD is a 208 amino acid protein consisting of an N-terminal Tnf receptor-associated factor (Traf)-binding consensus sequence and a C-terminal death domain (DD). The Traf-binding consensus sequence of EDARADD is used as a docking site for Traf1, Traf2, and Traf3, thereby recruiting Traf members and leading eventually to the activation of NF-κB [6]. The DD is involved in self-association of EDARADD and its interaction with EDAR [6,25]. Thus, EDARADD is central to Edar signaling. The N-terminal region is responsible for signal transduction and the C-terminal DD is required for receptor engagement.

To date, four *EDARADD* mutations have been found in a subset of human HED, one leads to autosomal dominant inheritance (Leu112Arg) [26], while the others lead to autosomal recessive inheritance (Glu142Lys, Pro121Ser, and Thr135-Val136del) [6,28,29]. All of these mutations are located in the DD and functional analyses showed that they resulted in the failure of EDARADD to interact with EDAR and to activate NF-κB. In the *crinkled* mouse, a genomic region of ~66-kb or more which includes exon 6 that encodes the entire DD, is deleted [25]. The *crinkled* mouse displays developmental defects in hair follicles, teeth, and sweat glands [30,31]. Hence, it is possible that a mutation in the DD of EDARADD is necessary for the HED syndrome to be manifested both in human and mouse.

All members of the DD superfamily form a highly compact structure comprising six antiparallel α-helix that is involved in homotypic and heterotypic protein-protein complex formation [32]. The region spanning the α1 to α4 helices of the DD of MyD88, a member of the death receptor superfamily, is required for its interaction with a downstream kinase [33]. A comparison of the amino acid sequences of the DD superfamily revealed that the Pro153-Ser missense mutation found in the present study is located in the α4 helix of the DD of EDARADD. This mutation may cause a profound change in the polarity of a crucial region and eventually diminish NF-κB signaling. It is likely that Pro153Ser affects the structure of the DD thereby interfering in the interaction of EDARADD with EDAR.

Mutations affecting the Eda pathway are known in medaka [13], zebrafish [14], mouse [4,6,8], cattle [15-18], dog [19], and human [3,5,6]. Of them, the mouse mutants have been widely characterized as a model organism of HED. Here we report the *swh* mutation as the first example of a mutation in the Eda pathway in the rat.

Because the rat is closely related to the mouse, it is important to recognize how the rat *Edaradd* mutant phenotype matches the mouse Eda pathway mutant phenotypes. Similar to the mouse mutants, the *swh/swh* rat displayed sparse hair, misshapen teeth, and absence of sweating. Additionally, like the Eda pathway mutant, the *swh/swh* rat had only abnormal awl hair in the coat. The *swh/swh* rat showed a lack of the ectoderm-derived glands, meibomian, preputial, and tongue. Interestingly, both serous and mucous glands were absent in the tongue of the *swh/swh* rat. This is a clear difference from the mouse Eda pathway mutants that lacked mucous glands but had serous glands in the tongue [34]. Moreover, in contrast to the complete absence of tail hair in the Eda pathway mutant mice, the *swh/swh* rat had hair on its tail. The penetrance of the kink tail phenotype was low in the *swh/swh* rat, while almost all Eda pathway mutant mice showed the kink tail. Lastly, the bald patch behind the ear was not present in the *swh/swh* rat, although it was a very characteristic phenotype of the Eda pathway mutant mice.

Why these phenotypes are different between the Eda pathway mutant mice and the *swh/swh* rats is yet to be explained. However, different types of mutations could possibly explain the differences. The mouse *crinkled* mutation is a deletion [6], while the *swh* mutation is missense. Although the Luc-reporter assay strongly suggested that *swh* is a null mutation, the possibility that *swh* might be a hypomorphic mutation cannot be eliminated because the activation of NF-κB found in the assay was very low. In the Eda pathway mutant mice, the mammary, salivary and tracheal submucosal glands have been well characterized [9,10]. Further analyses of these glands in *swh/swh* rats will give further insights into the functions of the Eda pathway genes in the development of these glands.

Conclusions

We successfully established the *swh/swh* rat as the first rat model of HED and identified *swh* as a Pro135Ser missense mutation in the *Edaradd* gene. The Pro135Ser mutant protein failed to activate NF-κB in the Eda signaling pathway. Thus, the *swh/swh* rat is a good model that can be used to investigate the pathological basis of HED.

Acknowledgements and Funding

The authors are grateful to the National BioResource Project for the Rat for providing the ACI/NKyo, WTC/Kyo, and WTC-*swh*/Kyo rat strains. This work was supported in part by the Grants-in-aid for Scientific Research from the Japan Society for the Promotion of Science (21300153 to TK) and by a Grant-in-aid for Cancer Research from the Ministry of Health, Labour and Welfare (to TK).

Authors' contributions

TK and MY performed the genetic and molecular biological experiments. RH and HH performed the histological examinations. TK wrote the paper and HH and TS revised the manuscript. All authors read and approved the final manuscript.

Received: 29 July 2011 Accepted: 21 October 2011
Published: 21 October 2011

References

1. Mikkola ML, Thesleff I: **Ectodysplasin signaling in development.** *Cytokine Growth Factor Rev* 2003, **14(3-4)**:211-224.
2. Salisbury DM, Stothers JK: **Hypohidrotic ectodermal dysplasia and sudden infant death.** *Lancet* 1981, **1(8212)**:153-154.
3. Kere J, Srivastava AK, Montonen O, Zonana J, Thomas N, Ferguson B, Munoz F, Morgan D, Clarke A, Baybayan P, *et al*: **X-linked anhidrotic (hypohidrotic) ectodermal dysplasia is caused by mutation in a novel transmembrane protein.** *Nat Genet* 1996, **13(4)**:409-416.
4. Srivastava AK, Pispa J, Hartung AJ, Du Y, Ezer S, Jenks T, Shimada T, Pekkanen M, Mikkola ML, Ko MS, *et al*: **The Tabby phenotype is caused by mutation in a mouse homologue of the *EDA* gene that reveals novel mouse and human exons and encodes a protein (ectodysplasin-A) with collagenous domains.** *Proc Natl Acad Sci USA* 1997, **94(24)**:13069-13074.
5. Monreal AW, Ferguson BM, Headon DJ, Street SL, Overbeek PA, Zonana J: **Mutations in the human homologue of mouse dl cause autosomal recessive and dominant hypohidrotic ectodermal dysplasia.** *Nat Genet* 1999, **22(4)**:366-369.
6. Headon DJ, Emmal SA, Ferguson BM, Tucker AS, Justice MJ, Sharpe PT, Zonana J, Overbeek PA: **Gene defect in ectodermal dysplasia implicates a death domain adapter in development.** *Nature* 2001, **414(6866)**:913-916.
7. Mikkola ML: **Molecular aspects of hypohidrotic ectodermal dysplasia.** *Am J Med Genet A* 2009, **149A(9)**:2031-2036.
8. Headon DJ, Overbeek PA: **Involvement of a novel Tnf receptor homologue in hair follicle induction.** *Nat Genet* 1999, **22(4)**:370-374.
9. Chang SH, Jobling S, Brennan K, Headon DJ: **Enhanced Edar signalling has pleiotropic effects on craniofacial and cutaneous glands.** *PLoS One* 2009, **4(10)**:e7591.
10. Melnick M, Phair RD, Lapidot SA, Jaskoll T: **Salivary gland branching morphogenesis: a quantitative systems analysis of the Eda/Edar/NFκB paradigm.** *BMC Dev Biol* 2009, **9**:32.
11. Gruneberg H: **The glandular aspects of the tabby syndrome in the mouse.** *J Embryol Exp Morphol* 1971, **25(1)**:1-19.
12. Gaide O, Schneider P: **Permanent correction of an inherited ectodermal dysplasia with recombinant EDA.** *Nat Med* 2003, **9(5)**:614-618.
13. Kondo S, Kuwahara Y, Kondo M, Naruse K, Mitani H, Wakamatsu Y, Ozato K, Asakawa S, Shimizu N, Shima A: **The medaka *rs-3* locus required for scale development encodes ectodysplasin-A receptor.** *Curr Biol* 2001, **11(15)**:1202-1206.
14. Harris MP, Rohner N, Schwarz H, Perathoner S, Konstantinidis P, Nusslein-Volhard C: **Zebrafish eda and edar mutants reveal conserved and ancestral roles of ectodysplasin signaling in vertebrates.** *PLoS Genet* 2008, **4(10)**:e1000206.
15. Drogemuller C, Distl O, Leeb T: **Partial deletion of the bovine *ED1* gene causes anhidrotic ectodermal dysplasia in cattle.** *Genome Res* 2001, **11(10)**:1699-1705.
16. Drogemuller C, Peters M, Pohlenz J, Distl O, Leeb T: **A single point mutation within the *ED1* gene disrupts correct splicing at two different splice sites and leads to anhidrotic ectodermal dysplasia in cattle.** *J Mol Med (Berl)* 2002, **80(5)**:319-323.
17. Ogino A, Kohama N, Ishikawa S, Tomita K, Nonaka S, Shimizu K, Tanabe Y, Okawa H, Morita M: **A novel mutation of the bovine *EDA* gene associated with anhidrotic ectodermal dysplasia in Holstein cattle.** *Hereditas* 2011, **148(1)**:46-49.
18. Gargani M, Valentini A, Pariset L: **A novel point mutation within the *EDA* gene causes an exon dropping in mature RNA in Holstein Friesian cattle breed affected by X-linked anhidrotic ectodermal dysplasia.** *BMC Vet Res* 2011, **7**:35.
19. Casal ML, Scheidt JL, Rhodes JL, Henthorn PS, Werner P: **Mutation identification in a canine model of X-linked ectodermal dysplasia.** *Mamm Genome* 2005, **16(7)**:524-531.
20. Kuramoto T, Morimura K, Nomoto T, Namiki C, Hamada S, Fukushima S, Sugimura T, Serikawa T, Ushijima T: **Sparse and wavy hair: a new model for hypoplasia of hair follicle and mammary glands on rat chromosome 17.** *J Hered* 2005, **96(4)**:339-345.
21. Saar K, Beck A, Bihoreau MT, Birney E, Brocklebank D, Chen Y, Cuppen E, Demonchy S, Dopazo J, Flicek P, *et al*: **SNP and haplotype mapping for genetic analysis in the rat.** *Nat Genet* 2008, **40(5)**:560-566.
22. Rothschild TC, Boylan ES, Calhoon RE, Vonderhaar BK: **Transplacental effects of diethylstilbestrol on mammary development and tumorigenesis in female ACI rats.** *Cancer Res* 1987, **47(16)**:4508-4516.
23. Kuramoto T, Kuwamura M, Tokuda S, Izawa T, Nakane Y, Kitada K, Akao M, Guenet JL, Serikawa T: **A mutation in the gene encoding mitochondrial Mg^{2+} channel MRS2 results in demyelination in the rat.** *PLoS Genet* 2011, **7(1)**:e1001262.
24. Reed WB, Lopez DA, Landing B: **Clinical spectrum of anhidrotic ectodermal dysplasia.** *Arch Dermatol* 1970, **102(2)**:134-143.
25. Yan M, Zhang Z, Brady JR, Schilbach S, Fairbrother WJ, Dixit VM: **Identification of a novel death domain-containing adaptor molecule for ectodysplasin-A receptor that is mutated in crinkled mice.** *Curr Biol* 2002, **12(5)**:409-413.
26. Bal E, Baala L, Cluzeau C, El Kerch F, Ouldim K, Hadj-Rabia S, Bodemer C, Munnich A, Courtois G, Sefiani A, *et al*: **Autosomal dominant anhidrotic ectodermal dysplasias at the EDARADD locus.** *Hum Mutat* 2007, **28(7)**:703-709.
27. Pispa J, Thesleff I: **Mechanisms of ectodermal organogenesis.** *Dev Biol* 2003, **262(2)**:195-205.
28. Chassaing N, Cluzeau C, Bal E, Guigue P, Vincent MC, Viot G, Ginisty D, Munnich A, Smahi A, Calvas P: **Mutations in *EDARADD* account for a small proportion of hypohidrotic ectodermal dysplasia cases.** *Br J Dermatol* 2010, **162(5)**:1044-1048.
29. Suda N, Bazar A, Bold O, Jigjid B, Garidkhuu A, Ganburged G, Moriyama K: **A Mongolian patient with hypohidrotic ectodermal dysplasia with a novel P121S variant in *EDARADD*.** *Orthod Craniofac Res* 2010, **13(2)**:114-117.

30. Kindred B: **The expression of the Tabby and crinkled genes in different genetic backgrounds in the mouse.** *Genetics* 1967, **55**(1):173-178.
31. Rao MS, Jaszczak E, Landis SC: **Innervation of footpads of normal and mutant mice lacking sweat glands.** *J Comp Neurol* 1994, **346**(4):613-625.
32. Weber CH, Vincenz C: **The death domain superfamily: a tale of two interfaces?** *Trends Biochem Sci* 2001, **26**(8):475-481.
33. Loiarro M, Gallo G, Fanto N, De Santis R, Carminati P, Ruggiero V, Sette C: **Identification of critical residues of the MyD88 death domain involved in the recruitment of downstream kinases.** *J Biol Chem* 2009, **284**(41):28093-28103.
34. Wells KL, Mou C, Headon DJ, Tucker AS: **Defects and rescue of the minor salivary glands in Eda pathway mutants.** *Dev Biol* 2011, **349**(2):137-146.

doi:10.1186/1471-2156-12-91
Cite this article as: Kuramoto *et al.*: A rat model of hypohidrotic ectodermal dysplasia carries a missense mutation in the *Edaradd* gene. *BMC Genetics* 2011 12:91.

Chapter XX

PolyADP-Ribosylation in Postfertilization and Genome Reprogramming: Implications for Carcinogenesis

Tomoharu Osada and Mitsuko Masutani

Additional information is available at the end of the chapter

http://dx.doi.org/10.5772/46097

1. Introduction

Pottranslational modification of proteins (PTM) is involved in molecular targeting or signal transduction as a basis of a variety of biological processes of the cells. Approximately 300 PTMs are existed in the cells, some of which are supposed to have important roles in cell physiology or embryogenesis. In addition, some modifications are reciprocally interacted, which regulates gene expression or protein dynamics or processing. We focus here polyADP-ribosylation (PARylation), which is found to contribute importantly at fertilization and postfertilization development. Moreover, we discuss the possible drug discovery of ADP-ribosylation inhibitors in carcinogenesis or fertility control.

Upon fertilization, two kinds of genetic materials meet together to generate a new organism [1]. Meanwhile, the organism develops without major expression of genes from genomes. Although maternal proteins are supposed essential for the period, the details are ill understood. Transition of zygotic gene expression is also essential for further development. Some PTMs on transcriptional factors may be key regulation to express the genes which supports early development. Parental DNAs are differently regulated in the postfertilized eggs, although the biological significance is controversial. Theses implications suggest importance of PTMs on postfertilization and transition of zygotic development. Recently we found that PARylation, a PTM of protein is important for postfertilization development, which seems similar with those of carcinogenesis.

The PARylation reaction is a PTM of proteins, which is synthesized with poly(ADP-ribose) polymerase (PARP) and metabolized with poly(ADP-ribose) glyceraldehyde (PARG) [2,3]. The reciprocal regulation is speculated as a key mechanism that underlies reversible

regulation of gene expression. The poly(ADP-ribose) is generated from NAD, an energy reservoir of the cells by PARP. The PARP synthesizes poly(ADP-ribose) using NAD. PARP polymerizes ADP-ribose residues to generate poly(ADP-ribose) chains onto proteins. PARylation reaction itself is regulated by auto-PARylation of Parp1. Since the ADP-ribose residue is negatively charged, the acceptor proteins become negatively charged by the addition of ADP-ribose residues. The electrical charge-shift of the protein induced by PARylation may decrease an easy access of proteins into the DNA structure or may induce structural instability of protein-DNA interactions, because the negative charge of poly(ADP-ribose) supports its association with DNA-binding proteins, which are positively charged. The recognition of DNA sequences by protein structure may also be affected by PARylation. Upon postfertilization development, zygotic gene expression is essentially activated prior to the 4-cell cleavage stage in mice and human. Therefore, behavior of maternal molecules plays important roles at postfertilization development before zygotic gene activation. PTM of protein is supposed to contribute to protein dynamics at postfertilization development. Pharmacological blockage of PARylation revealed defects of postfertilization development in mice [4]. The data raise a question regarding the roles of PARylation at fertilization development. A wealth of study revealed that NAD is rich in eggs and rapidly degraded upon fertilization in Xenopus larvae. Parp activation at fertilization may contribute to consumption of NAD, which may bring a plausible explanation towards the uncovered subject. Postfertilization development is specific biological window to highlight the significance of PTM, because transcription is minor mechanisms for the organisms at the period. In this chapter, we discuss the roles of PARylation in eggs and the function of postfertilization development. Further we discuss the possible implications to drug discovery focusing on PARylation regulation. We focus on polyADP-ribosylation because we previously showed that no fertilized eggs were obtained by pharmacological blockage of PARylation by a PARP inhibitor, PJ-34 [4]. Other inhibitors of PARylation showed similar results. Therefore, a hypothesis was raised that posttranslational regulation is key regulation of maternal genetic materials at fertilization because no robust transcription is occurred at the beginning of life.

2. PARylation in postfertilization development

Recent research showed that pharmacological blockage of PARylation leads to defects in pronuclear fusion during postfertilization in mice. Based on the observations, several approaches were achieved to investigate the roles of PARylation in vivo and mechanisms of reprogramming applicable for regenerative medicines or elucidation of human diseases including carcinogenesis.

Based on our observations regarding the disorganized microtubule assembly in oocytes by PARylation inhibitors, polyADP-ribosylated proteins of oocytes and postfertilized eggs were searched. We found that the tubulins (α1c, β2c) [4] and glutathione *S*-transferees μ5 (GSTμ5) (Osada et al., unpublished data) was highly polyADP-ribosylated after fertilization.

Because PARylation is known as a regulatory machinery of DNA surveillance system, this data provided us with a novel sight of view on the roles of PARylation regarding cell signaling and metabolisms. As a major upstream signaling cascade after sperm entry, MAP-kinase (MAPK) signaling has been postulated as the key regulatory mechanism for pronucleus formation, and Parp1 is reported to be involved in the regulation of MAPK signaling [5]. Our data suggest that Parp1 is a novel nuclear component for PPN (Pseudo pronuclei) formation, which may be mediated by MAPK signaling. Phosphorylation level of Erk was decreased in the MII phase of Parp-1 null oocyte. Because the downregulation of Erk phosphorylation is known to disturb microtubule organization, these results raise a possibility that the transient administration of a Parp inhibitor may block the early phase of post-fertilization process.

Second, we focused on the roles of polyADP-ribosylation on epigenetic regulation. Accumulating study suggests that PARylation has a fundamental role in transcription as well as DNA surveillance, which mediates topological changes of the DNA structure [6,7]. We first examined the effects of PARylation on chromatin modification during postfertilization development. An immunofluorescence study using histone acetylation and methylation antibodies were initially carried out. Upregulation of dimethyl-H3k4 in the PARylation-inhibited embryos at 6 hpf, and downregulation of dimethyl-H3K9 and dimethyl-H3K27 at 15 hpf were observed (unpublished data, Osada et al.). Recently, functional links between histone methylation and DNA methylation have been elucidated. Based on our observations of distinct effects of PARylation inhibition on histone modification regulation, we next sought for the roles of PARylation in DNA methylation. Global methylation of the maternal genome is maintained and sperm DNA is quickly demethylated during the postfertilization period [8]. The low immunoreactivity to the MetC antibody in the PARylation inhibited embryos was observed and it persisted at least until 15 hpf (unpublished data, Osada et al.). The data suggest that epigenetic regulation is asymmetrically activated during postfertilization development, although gene expression is not activated. Therefore, PARylation affects the integrity of epigenetic regulation of oocytes and postfertilized eggs (Figure 1).

An additional implication of this finding is that PARylation regulates the epigenetic nonequivalence of the pronuclei in mice. The molecular mechanisms regulating the asymmetric DNA methylation of one-cell embryos are largely unknown, and we showed that PARylation is involved in the epigenetic regulation of the mouse early development. PGC7/Stella-deficient eggs show similar defects in the protection of female pronuclei from DNA demethylation [9]. The nucleo-cytoplasmic transport of the responsible proteins appears to be important for the regulation of DNA methylation. The role of PARylation in DNA methyltransferase (DMNT) regulation is yet to be fully elucidated, although the interaction of DNMT1 with PARP1 and the indirect repression of DNMT1 activity by interacting with PAR have been suggested [10]. Based on our data showing an association between PARylation or PARP and histone modification, it is speculated that PARylation

may regulate the accessibility of DNMT or demethylase to DNA, in a manner mediated by chromatin remodeling. Our study provides a novel avenue for better understanding of establishment of chromatin organization through the histone codes and DNA methylation that may underlie at the beginning of zygotic development.

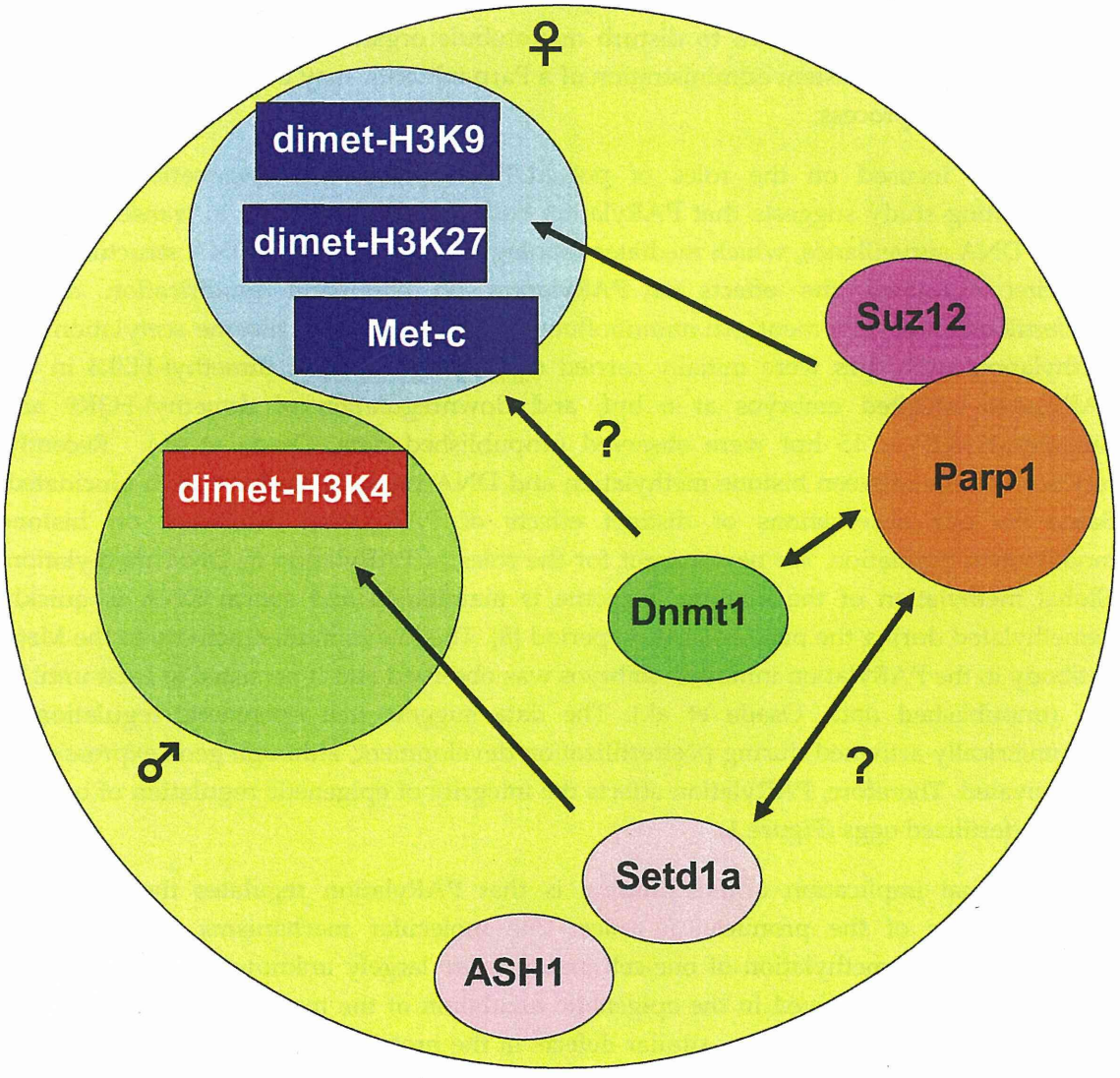

Figure 1. Scheme of putative roles of PARylation in the chromatin dynamics of one-cell embryos. In the one-cell embryos (yellow circle), PARP1 may interact with histone modifying enzymes including Suz12, that might affect the asymmetric regulation of histone modifications in the pronuclei (male pronucleus in blue circle and female pronucleus in green).

To examine whether there is a direct or indirect linkage of epigenetic regulation with PARylation, we screened molecules that interacts with Parp1. To elucidate the molecular basis of the effect of PARylation on histone modification, we performed yeast two-hybrid screening using the bait vector carrying N-terminal and automodification domain. The Suz12, a histone methyltransferase, was identified as a candidate molecule interacting with Parp1 (unpublished data, Osada et al.). Suz12 is a component of PRC2/3/4 (Polycomb Repressive Complex 2/3/4), which regulates the repressive status of transcription by the methylation of histone H3K9 and H3K27. Our findings support the idea that Parp1 acts as a regulatory scaffold for the access of PRC2/3 to target DNA, because none of the components of the PRC2/3/4 complexes are DNA binding proteins. OCT4, bidirectional transcriptional regulator, is suggested to play a role of transcriptional regulation by recruiting PRC2/3/4 to the target genes, which are indispensable for the embryonic development. Modification of PARylation triggers loosening of chromatin structure, which may enable the access of transcriptional factors to DNA duplex structure.

Third, as shown in Figure 2, defects in pronuclear formation by inhibition of PARylation raise a possibility that PARylation is involved in laminar formation of pronuclei [4]. In fact, HP1, an anchor protein of lamina and heterochromatin is polyADP-ribosylated [11]. Our findings showed prolonged presence of lamin-A/C, a core protein of lamina by PARP inhibitor PJ-34 treated eggs. Interestingly, lamin-A/C is predominantly existed in undifferentiated cells. Lamin-A/C is known as a marker of carcinogenesis [4]. Our observation provided a new insight into regulatory machinery of laminar formation in pluripotent cells by PARylation. Our initial data suggest that cell-cycle is not disturbed when embryos were subjected to treatment of PARP inhibitor.

During the first cell cycle of mouse embryos, a few genes are transcribed mainly from paternal genome. Inhibition of transcription during one-cell embryos by RNA polymerase inhibitors showed dispensable roles of transcription in normal development. Zygotic gene activation is required for progression from 2-cell to 4-cell embryos. These indicate that posttranslational regulation of protein should act as a stem mechanism of the development of one-cell embryos. Upon fertilization, highly compacted chromatin of gametes was acutely decondensed to form pronuclei (PN) within a few hours. Protamines of sperm chromatin are replaced by maternal histone H1 during this process, which may be associated with global hypomethylation of sperm-derived PN. In contrast, maternal chromatin arrested at metaphase II progresses rapidly into G1 phase and subsequently forms the female PN. DNA synthesis from paternal genome is preceded to that from maternal DNA. A minor transcription is activated solely from male PN. This evidence suggests that the requirement for the posttranslational regulations of parental genomes before mingling of both gamete DNA to begin the proper zygotic development. Of posttranslational modification of proteins, we examined here the effects of PARylation during the first cell cycle of mouse embryos. Metabolism of NAD, which is the substrate of PARPs, is acutely activated upon fertilization. Further analysis will elucidate the biological functions of PARylation upon fertilization and downstream target molecules of them.

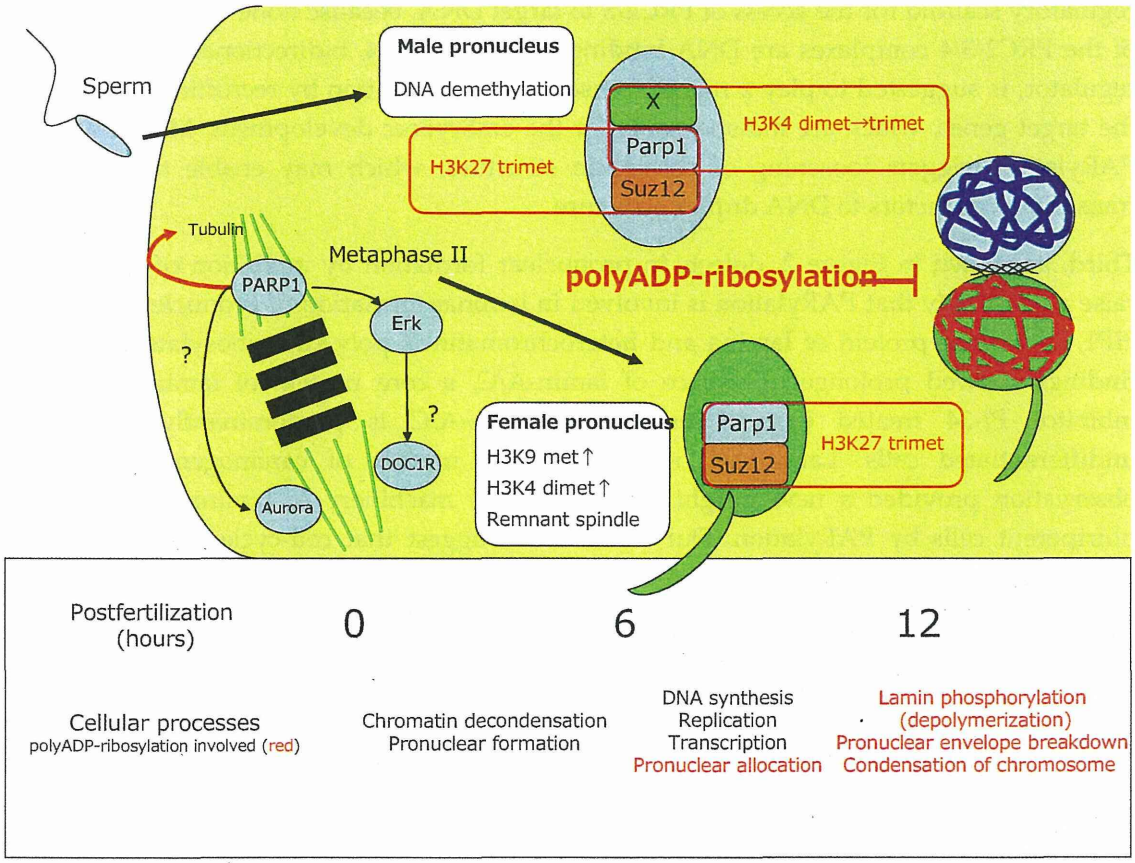

Figure 2. Model for regulation of pre- and postfertilization process by PARylation. Biological processes occurred during pre- and postfertilization were shown. Putative correlation with polyADP-ribosylation were indicated in red.

3. Implication towards reprogramming

In 1997, the first cloned animals were generated [12]. Cytogenetic analyses have shown that karyotypic aberrations occur in cloned embryos during the first mitotic cleavage. Epigenetic errors in cloned animals are also argued to be the major reason for the limited success rates of cloned animal births. However, whether genome-wide chromatin remodeling during nuclear reprogramming causes DNA damage, or whether defects in DNA repair cause the inefficiency of cloned animal births have not been investigated. Recently, it was reported that double strand break (DSB)–mediated chromatin remodeling regulates transcription, and that Parp1 is critically involved in this process. Various roles for Parp1 have been described, including in the chromatin remodeling involved in transcriptional regulation [2,3]. The roles of Parp1 in NT-embryo development in the contexts of DNA repair and chromatin remodeling was examined. To do this, we used *Parp1*-null mutant cells as recipient oocytes and as a source of donor nuclei.

We observed that the activation process in NT eggs was enhanced in *Parp1*–null NT embryos, although some genomic instability was observed (Osada T., unpublished data). Dynamic changes in histone acetylation and methylation were induced under *Parp-1* deficiency in NT embryos (Figure 3). The lack of Parp1 may thus facilitate chromatin condensation or transcriptional silencing. Parp1 is involved in both the regulation of DNA strand break repair and the epigenetic control of gene expression. Our findings suggest that Parp1 is important for chromatin remodeling possibly through histone modification during the nuclear reprogramming of NT embryos. The phosphorylation of histone H2AX at DSBs is believed to be crucial for the recognition and repair of DNA damage. The foci-like presence of γH2AX in the NT embryos implied that DNA repair was taking place in the PNN. H2AX is a direct target of ATM kinase, which is expressed at the spindle of MII oocytes, and Parp1 interacts with ATM. The prolongation of the γH2AX foci in the *Parp1*$^{-/-}$ NT embryos could therefore be related to a delay in repairing DNA strand breaks, as is the case with *Parp1*$^{-/-}$ MEF and ES cells, which show prolonged γH2AX foci after DNA damage induced by neocartinostatin. In *Parp1*$^{-/-}$ NT embryos, mitotic arrest of embryogenesis at the 2-4-cell stage was frequently observed, accompanied by polynucleated blastomeres. Since Parp1 is located in centrosomes as well as in nuclei, the lack of Parp1 may have disturbed the normal cell division cycle and the synchronous pattern of cell division among the blastomeres. Transient Parp-1 functional inhibition may be therefore useful to improve the efficiency of NT by modulating the dynamic organization of chromatin without causing genomic instability.

4. Implication towards human diseases

PARylation has been known to possess important roles in carcinogenesis. PARP mainly affects DNA surveillance system in the cells, which deficit increases the risk of carcinogenesis. In addition, recent study showed a functional relationship between PARP